ijrr

The International Journal of Robotics Research
30(6) 647–658

DOI: 10.1177/0278364910394227
ijr.sagepub.com
SAGE

Modeling, control and experimental characterization of microbiorobots

Mahmut Selman Sakar[1], Edward B Steager[1], Dal Hyung Kim[2], A Agung Julius[3], MinJun Kim[2], Vijay Kumar[1] and George J Pappas[1]

Abstract

In this paper, we describe how motile microorganisms can be integrated with engineered microstructures to develop a micro-bio-robotic system. SU-8 microstructures blotted with swarmer cells of Serratia Marcescens *in a monolayer are propelled by the bacteria in the absence of any environmental stimulus. We call such microstructures with bacteria MicroBioRobots (MBRs) and the uncontrolled motion in the absence of stimuli self actuation. Our paper has two primary contributions. First, we demonstrate the control of MBRs using self actuation and DC electric fields, and develop an experimentally validated mathematical model for the MBRs. This model allows us to use self actuation and electrokinetic actuation to steer the MBR to any position and orientation in a planar micro channel. Second, we combine our experimental setup and a feedback control algorithm to steer robots with micrometer accuracy in two spatial dimensions. We describe the fabrication process for MBRs and show experimental results demonstrating actuation and control.*

Keywords

Microrobot, wireless, untethered, bacterial actuation, electrokinetic actuation, stochastic model, visual servoing, biomedical, in vitro.

1. Introduction

The independent manipulation of cells and man-made objects on the micrometer scale in a controlled manner using autonomous microstructures is one of the great challenges in microscale engineering. Actuation can be realized using inorganic components and there is extensive ongoing research on developing artificially engineered micro/nanoscale structures with novel approaches of microactuation (Chang et al., 2007; Dauge et al., 2007; Donald et al., 2008; Dreyfus et al., 2005; Ghosh and Fischer, 2009; Jager et al., 2000; Leong et al., 2009; Pawashe et al., 2009; Vollmers et al., 2008; Zhang et al., 2009). There is relatively little work on exploiting naturally-occurring biomolecular motors for actuation of micro and nano structures. Biomolecular motors can be used for actuation, but these systems are difficult to employ when isolated from the supporting cells (Feinberg et al., 2007; van den Heuvel and Dekker, 2007). The use of microorganisms to produce useful work has been previously demonstrated by a number of different groups (Darnton et al., 2004; Hiratsuka et al., 2006; Sokolov et al., 2010; Weibel et al., 2005). The potential for developing microrobots powered by bacteria has been demonstrated by several researchers (Behkam and Sitti, 2007; Martel et al., 2006; Steager et al., 2007).

Our paper builds on our previous work (Steager et al., 2007) on bacterial actuation to develop an integrated micro-bio-robotic system. SU-8 microstructures blotted with swarmer cells of *Serratia marcescens* in a monolayer are propelled by the bacteria in the absence of any environmental stimulus. We call these microstructures with bacteria *MicroBioRobots* (MBRs) and the uncontrolled motion *self actuation*. In the first part of the paper, we construct a stochastic mathematical model for the self actuation, based on the assumption that the behavior of each bacterium is

[1]School of Engineering and Applied Sciences, University of Pennsylvania, USA
[2]Department of Mechanical Engineering and Mechanics, Drexel University, USA
[3]Department of Electrical, Computer and Systems Engineering, Rensselaer Polytechnic Institute, USA

Corresponding author:
Mahmut Selman Sakar, GRASP Laboratory, School of Engineering and Applied Sciences, University of Pennsylvania, Philadelphia, PA 19104, USA.
Email: sakarmah@seas.upenn.edu

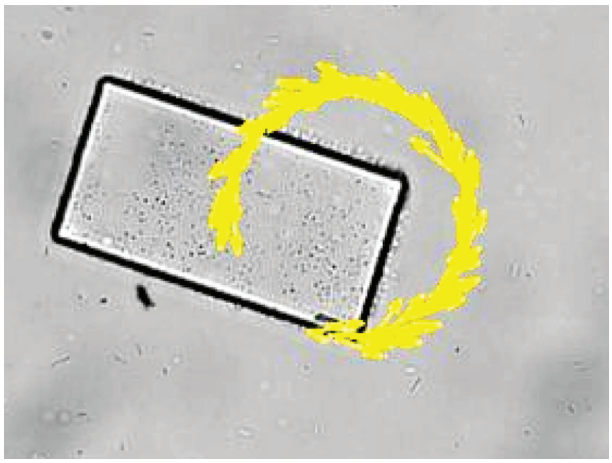

Fig. 1. A rectangular MBR (50 μm $\times$ 100 μm) that is used in this paper. The computer vision tracking system marks the trajectory of the MBR and its computed interframe velocity with the arrows (Julius et al., 2009).

random and independent of that of its neighbors. The study of actuation by using a large number of random actuators has been reported elsewhere (Ueda et al., 2007). In addition to developing the stochastic model, we also perform parameter identification for the model, based on experimental data. We then demonstrate that the model with the estimated parameters is able to predict the behavior of the system very well. One of the key findings is that although the system is inherently distributed, in the sense that there are a large number of independent actuators, we can construct an accurate model with only a few parameters representing the distribution of the bacteria.

In the second part of the paper, we demonstrate the control of MBRs using DC electric fields, and develop an experimentally validated mathematical model for the MBRs. This model allows us to steer the MBR to any position and orientation in a planar micro channel using visual feedback from an inverted microscope. We employ a vision-based electrokinetic control strategy to steer robots by adjusting the applied voltage at each time step according to where they are and where they should be. We demonstrate that our approach allows us to steer MBRs along arbitrary trajectories in an autonomous fashion. The control algorithm steers the robots along their desired paths even if the properties of the robots (their charge, size and shape) and the properties of the fluid (pH, zeta potential, temperature) are not known precisely. We also characterize the overall system performance by applying sinusoidal control voltages to the system with varying frequencies. The method is wireless and non-invasive, and the entire system can be miniaturized further.

The remainder of this paper is organized as follows. In Section 2, we present the experimental methods for system operation. We present the stochastic mathematical model for the self actuation in Section 3 and the model for electrokinetic actuation in Section 4. The feedback control

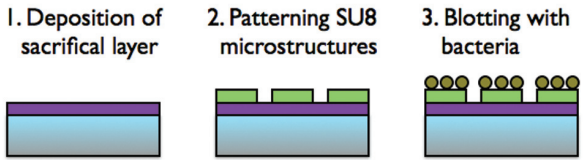

Fig. 2. Microstructure fabrication processes. See Section 2.

architecture is presented in Section 5, followed by the proposed control algorithm as well as a comparison of experimental and simulation results in section 6. We discuss the results in Section 7 and conclude the paper with Section 8, where we present a few potential future research directions.

2. Materials and methods

2.1. Fabrication of patterned microstructures

The SU-8 microstructures are patterned on 43mm $\times$ 50 mm glass slides with a thickness of 170 μm (No. 0). The fabrication sequence is shown in Figure 2. First, a spin-coating procedure was used to prepare the water-soluble sacrificial dextran layer (Linder et al., 2005). Next, a 5 μm layer of SU-8 Series 2 was spin-coated. The substrate was simply dried with nitrogen after Propylene Glycol Monomethyl Ether Acetate (PGMEA) development to protect the sacrificial layer from etching. Microstructures are automatically released when exposed to any source of water.

2.2. Bacterial strains, growth conditions and media

The bacteria *S. marcescens* are cultured using a swarm plate technique (LB broth containing 0.6% Difco Bacto-agar and 5 g/l glucose) as described in Darnton et al. (2004). Swarming bacteria are especially useful as actuators due to their power and size (Alberti and Harshey, 1990). These bacteria are hyperflagellated, elongated, and migrate cooperatively (Henrichsen, 1972). In addition, unlike some other types of bacteria, *S. marcescens* is not pathogenic. Bacteria were attached by blotting microstructures directly along the active swarm edge. The pink slime produced by swarmer cells of *S. marcescens* allows them to stick to the surface of the microstructures naturally.

2.3. Fabrication of experimental chamber

All experiments were conducted in a polydimethylsiloxane (PDMS) chamber on a 50$\times$50 mm^2 glass plate (see Figure 3). DC electric fields (EFs) were applied to the MBRs via agar salt bridges, Steinberg's solution (60 mM NaCl, 0.7 mM KCl, 0.8 mM $MgSO_4 \cdot 7H_2O$, 0.3 mM $CaNO_3 \cdot 4H_2O$) and graphite electrodes. It has been shown that salt bridges avoid contamination of possible electrode byproducts by successfully applying electric fields to a variety of cell types using similar devices (Tandon et al., 2009). They also

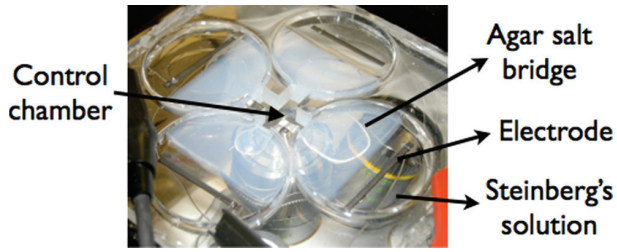

Fig. 3. Photograph of the experimental setup. All experimental observations were performed in the central portion of the control chamber.

keep bubbles formed around electrodes outside the control chamber. The temperature, calcium level and pH are normally very stable inside the chamber within the 1-hour duration of experiments (Song et al., 2007). This design was optimized to apply EFs efficiently in multiple directions. In order to minimize the possible adverse effects of electrode byproducts, we used graphite electrodes. The electrodes were fixed in parallel horizontal positions inside the compartments filled with Steinberg's solution to generate uniform EFs all over the control chamber. The control chamber was filled with motility buffer (0.01 M potassium phosphate, 0.067 M sodium chloride, 10^{-4} M ethylenediaminetetraacetic acid (EDTA), and 0.002% Tween-20, pH 7.0). Observations were performed in the central portion of the control chamber where dielectrophoretic effects due to field nonlinearities are minimized.

Voltages were applied to the control chamber through a National Instruments PCI-6713 analog output board. Two analog output channels were routed to two single channel Ametek XTR 100-8.5 amplifiers using the analog programming mode in conjunction with isolated connectors. Two additional analog output channels were used to control double pole, double throw (DPDT) switches, which functioned to reverse the polarity of the system.

2.4. *Image processing and feedback control*

A tracking algorithm was designed to analyze the motion of the MBRs in the motility buffer. The current study analyzed two distinct motions of rigid bodies: translation and rotation. To characterize the motion of the bacteria-driven microstructures, the geometric centroid and orientation angle was traced. Imaging was performed on a Leica DMIRB inverted microscope using phase contrast. Video was captured using a high-speed camera (MotionPro X3, Redlake). A tracking algorithm was designed to analyze the motion of the geometric centroid. Frames of video were captured, digitized and imported directly into MATLAB for analysis. The grayscale images were converted to binary images using a threshold tuned to optimize the effect of edge contrast of the SU-8 microstructure. The binary images were then inverted and all closed regions were filled. Closed structures of all sizes were next identified as individual elements, and elements smaller and larger than a predetermined pixel count were deleted leaving the area of the microstructure clearly defined and isolated. Finally, microstructure centroid location and orientation for each frame were determined and written to a data file. This data file was passed to the control algorithm for further analysis.

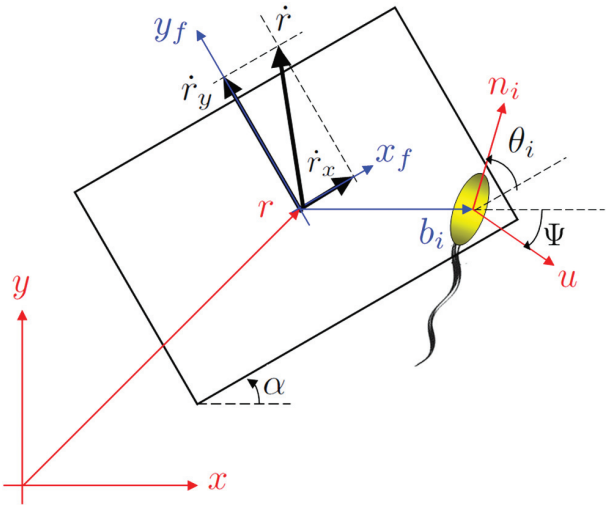

Fig. 4. A schematic of an MBR. The angle α is formed by the main axis of the MBR and the x-axis. The vector $\mathbf{r}$ denotes the position of the MBR's center of mass. The vector $\mathbf{b}_i$ denotes the position of the ith bacterium with respect to the MBR's center of mass. The vector n_i is a unit vector that denotes the orientation of the ith bacterium. The angle θ_i is formed by the MBR's main axis and the orientation of the ith bacterium.

3. Model for self actuation

There are two approaches to actuating an MBR, *self actuation* and electrokinetic actuation. Self actuation is due to the random swimming and tumbling action of individual cells. In this section, we introduce a stochastic kinematic model for the self actuation. A version of this model has appeared previously in our conference publication (Julius et al., 2009).

3.1. *Stochastic kinematic model*

The state of the MBR is characterized by its position on the plane and its orientation. See Figure 4 for an illustration. We define the vector $\mathbf{r} = (x, y)$ to be the planar position of the MBR's center of mass. The orientation of the MBR is characterized by the angle α, which is formed by the main axis of the MBR and the x-axis of the inertial coordinate frame.

We assume that there are N_b bacteria attached to a MBR. The position of the ith bacterium with respect to the center of mass of the MBR is denoted by the vector $\mathbf{b}_i = (b_{i,x}, b_{i,y})$ in the body-fixed coordinate frame, and its orientation is characterized by the angle θ_i. We also define the amount of (time varying) propulsive force provided by the ith bacterium as $p_i(t)$.

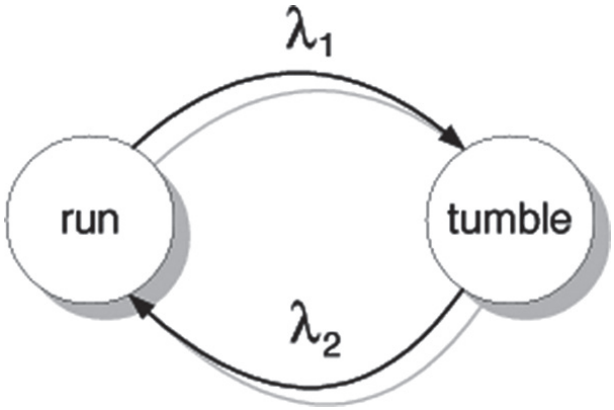

Fig. 5. A two-state continuous Markov chain model for the stochastic behavior of the bacteria. The transition rates between the states are given as λ_1 and λ_2.

The equation of translational motion of the MBR is given by

$$M\frac{d^2\mathbf{r}}{dt^2} = \sum_{i=1}^{N_b} p_i n_i - k_T \frac{d\mathbf{r}}{dt}, \tag{1}$$

where M is the total mass of the MBR system (including the bacteria), n_i is the unit vector in the inertial coordinate frame that represents the orientation of the ith bacterium, and k_T is the translational viscous drag coefficient. Similarly, the rotational motion can be characterized by

$$I\frac{d^2\alpha}{dt^2} = \sum_{i=1}^{N_b} p_i \cdot \left(b_{i,x}\sin\theta_i - b_{i,y}\cos\theta_i\right) - k_R\frac{d\alpha}{dt}, \tag{2}$$

where I is the total moment of inertia of the MBR system and k_R is the rotational viscous drag coefficient. In an environment with very low Reynolds number, the inertia effect is negligible, i.e. $k_T \gg M,\ k_R \gg I$.

Consequently, the translational and the rotational accelerations are negligible. Therefore, (1) and (2) can be accurately replaced with

$$\frac{d\mathbf{r}}{dt} = \frac{1}{k_T}\sum_{i=1}^{N_b} p_i n_i, \tag{3a}$$

$$\omega := \frac{d\alpha}{dt} = \frac{1}{k_R}\sum_{i=1}^{N_b} p_i \cdot \left(b_{i,x}\sin\theta_i - b_{i,y}\cos\theta_i\right). \tag{3b}$$

The propulsion forces, $p_i(t)$, are stochastic processes. Empirical observations by Berg (2000) reveal that, in the absence of chemotactic chemical agents, the process can be accurately modeled as a continuous-time Markov chain (Cassandras and Lafortune, 1999) with two states, *run* and *tumble*, where $\lambda_1 = 1\ \mathrm{s}^{-1}$ and $\lambda_2 = 10\ \mathrm{s}^{-1}$ (see Figure 5). Therefore, under these conditions, the ratio between run and tumble is 10 to 1. We assume that during *tumble*, a bacterium does not provide any propulsion, while during *run* it delivers the maximal propulsive force of $p_{\max} = 0.45$ pN reported in the literature (Darnton et al., 2007).

If we define $\phi(t) = (\phi_1(t), \phi_2(t))^T$ as the probability of finding the system in the *run* and *tumble* state at time t, the evolution of $\phi(t)$ is given by

$$\frac{d}{dt}\begin{bmatrix}\phi_1\\ \phi_2\end{bmatrix} = \begin{bmatrix}-\lambda_1 & \lambda_2\\ \lambda_1 & -\lambda_2\end{bmatrix}\begin{bmatrix}\phi_1\\ \phi_2\end{bmatrix}. \tag{4}$$

From here, it follows that any initial distribution $\phi(0)$ converges exponentially to a steady state distribution given by

$$\begin{bmatrix}\phi_1(\infty)\\ \phi_2(\infty)\end{bmatrix} = \begin{bmatrix}\frac{\lambda_2}{\lambda_1+\lambda_2}\\ \frac{\lambda_1}{\lambda_1+\lambda_2}\end{bmatrix}. \tag{5}$$

3.2. Quantitative analysis of the MBR rotation

If we denote the parameter

$$c_i := \frac{b_{i,x}\sin\theta_i - b_{i,y}\cos\theta_i}{k_R}, \tag{6}$$

then the orientation of the MBR α satisfies the relation

$$\alpha(t) = \alpha(0) + \int_0^t \sum_{i=1}^{N_b} c_i \cdot p_i(\tau)\ d\tau. \tag{7}$$

From here, we can compute the expectation of $\alpha(t)$ as

$$E(\alpha(t)) = \alpha(0) + \bar{p}\sum_{i=1}^{N_b} c_i t. \tag{8}$$

Here we use the assumption that at the beginning of the time interval of interest, $t = 0$, the processes $p_i(t)_{i=1\ldots N_b}$ have reached their steady state. In that case, their expectation is then given by the steady state expected value, $\bar{p}$, which can be computed as

$$\bar{p} = \frac{\lambda_2}{\lambda_1+\lambda_2}\cdot p_{\max} = 0.41\ \text{pN}. \tag{9}$$

Similarly, we can compute the variance of $\alpha(t)$ as follows:

$$\begin{aligned}\mathrm{Var}(\alpha(t)) &= E\left(\int_0^t \sum_{i=1}^{N_b} c_i \cdot (p_i(\tau) - \bar{p})\ d\tau\right)^2,\\ &= E\left(\int_0^t\int_0^t \sum_{i=1}^{N_b} c_i \cdot (p_i(\tau)-\bar{p}) \sum_{j=1}^{N_b} c_j \cdot \left(p_j(\eta)-\bar{p}\right)\ d\tau\ d\eta\right),\\ &= \int_0^t\int_0^t \sum_{i=1}^{N_b}\sum_{j=1}^{N_b} c_i \cdot c_j \cdot \left(E\left(p_i(\tau)p_j(\eta)\right) - \bar{p}^2\right)\ d\tau\ d\eta. \end{aligned} \tag{10}$$

Assuming that the random behavior of the bacteria are independent one from another, we can simplify (10) into

$$\mathrm{Var}(\alpha(t)) = 2\int_0^t\int_\eta^t \sum_{i=1}^{N_b} c_i^2 \cdot \left(E\left(p_i(\tau)p_i(\eta)\right) - \bar{p}^2\right)\ d\tau\ d\eta. \tag{11}$$

Table 1. The joint probability density function $P\{(p_i(\tau) = A, p_i(\eta) = B\}$.

$A\backslash B$	$p_{\max}$	0
$p_{\max}$	$\frac{\lambda_2^2+\lambda_1\lambda_2 e^{(\lambda_1+\lambda_2)(\eta-\tau)}}{(\lambda_1+\lambda_2)^2}$	$\frac{\lambda_1\lambda_2-\lambda_1\lambda_2 e^{(\lambda_1+\lambda_2)(\eta-\tau)}}{(\lambda_1+\lambda_2)^2}$
0	$\frac{\lambda_1\lambda_2-\lambda_1\lambda_2 e^{(\lambda_1+\lambda_2)(\eta-\tau)}}{(\lambda_1+\lambda_2)^2}$	$\frac{\lambda_1^2+\lambda_1\lambda_2 e^{(\lambda_1+\lambda_2)(\eta-\tau)}}{(\lambda_1+\lambda_2)^2}$

Furthermore, using the assumption mentioned above that the processes have reached the steady state at $t = 0$, we can compute $E\left(p_i(\tau)p_i(\eta)\right)$ through the Bayesian formula. The values of $P\{(p_i(\tau) = A), (p_i(\eta) = B)\}$ are given in Table 1.

We can compute that

$$E\left(p_i(\tau)p_i(\eta)\right) = \frac{\lambda_2^2 + \lambda_1\lambda_2 e^{(\lambda_1+\lambda_2)(\eta-\tau)}}{(\lambda_1+\lambda_2)^2} p_{\max}^2, \tag{12}$$

and

$$\mathrm{Var}(\alpha(t)) = \frac{2\lambda_1\lambda_2 p_{\max}^2}{(\lambda_1+\lambda_2)^3}\sum_{i=1}^{N_b} c_i^2 \cdot \left(t - \frac{1-e^{-(\lambda_1+\lambda_2)t}}{\lambda_1+\lambda_2}\right). \tag{13}$$

From (13) we see that both the expectation and the variance of $\alpha(t)$ grow asymptotically linearly. The standard deviation of $\alpha(t)$ grows asymptotically with $\sqrt{t}$, which is half an order slower than the expectation. Consequently, as $t \to \infty$, the ratio of the standard deviation to the expectation goes to 0. This means the expectation can be used as a good estimate of the steady state behavior of the system. The expectation of $\alpha(t)$ predicts that the MBR undergoes a steady rotation as a steady state behavior. In the next section, we will see that this is justified by the experimental results (see Figure 7(a)).

Notice that the assumption that the random behavior of the bacteria are independent one from another is not essential in deriving this result. To see this, consider the extreme case, where all the bacteria are perfectly correlated. In this case, the term $\sum_{i=1}^{N_b} c_i^2$ in (13) will be replaced by $\sum\sum_{i,j=1}^{N_b} c_i c_j$, which does not change the conclusion.

3.3. Parameter estimation

The components of the translational velocities on the axis of the body fixed coordinate frame (see Figure 4) are

$$v_x := \dot{r}_x = \frac{1}{k_T}\sum_{i=1}^{N_b} p_i \cos\theta_i,\ v_y := \dot{r}_y = \frac{1}{k_T}\sum_{i=1}^{N_b} p_i \sin\theta_i. \tag{14}$$

Their respective expectations are then given by

$$E(v_x) = \frac{\bar{p}}{k_T}\sum_{i=1}^{N_b}\cos\theta_i,\ E(v_y) = \frac{\bar{p}}{k_T}\sum_{i=1}^{N_b}\sin\theta_i. \tag{15}$$

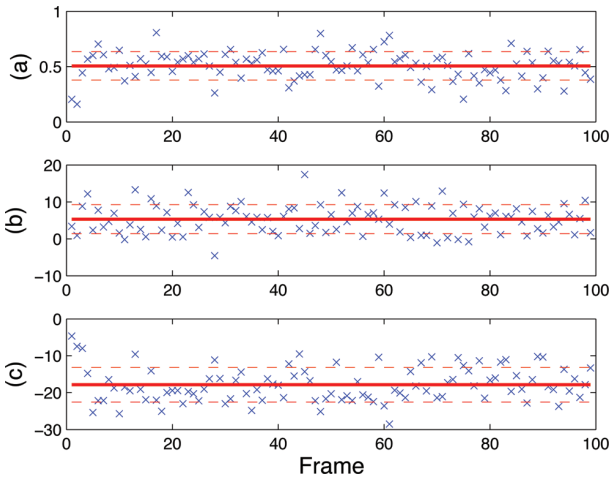

Fig. 6. The computed data for a rectangular MBR (50 μm $\times$ 100 μm). (a) $\{\bar{\omega}_i\}$ in rad/s, (b) $\{\bar{v}_{x,i}\}$ in μm/s, (c) $\{\bar{v}_{y,i}\}$ in μm/s. The solid lines show the averages of the data, while the gaps between the solid lines and the dashed lines represent the standard deviations.

From (3b), we can obtain the expectation of the angular velocity of the MBR, which is given by

$$E(\omega) = \frac{\bar{p}}{k_R}\sum_{i=1}^{N_b}\left(b_{i,x}\sin\theta_i - b_{i,y}\cos\theta_i\right). \tag{16}$$

It is clear from (14)–(16) that the expected velocities only depend on three parameters:

$$\beta_1 := \frac{1}{k_T}\sum_{i=1}^{N_b}\cos\theta_i,\ \beta_2 := \frac{1}{k_T}\sum_{i=1}^{N_b}\sin\theta_i,$$

$$\beta_3 := \frac{1}{k_R}\sum_{i=1}^{N_b}\left(b_{i,x}\sin\theta_i - b_{i,y}\cos\theta_i\right).$$

We estimate the values of these parameters using experimental data. We extract frames from the video taken during the experiment. In each frame, the position and orientation of the MBR are identified using digital image processing. As the results, we have three time series $\{\bar{x}_i\}$, $\{\bar{y}_i\}$, and $\{\bar{\alpha}_i\}$, with $i = 1, \ldots, N$, consisting of the planar position of the MBR and its orientation in N frames. The body fixed coordinate components of the MBR's translational velocity at the ith frame can be approximated using the forward difference method to give

$$\begin{bmatrix} \bar{v}_{x,i} \\ \bar{v}_{y,i} \end{bmatrix} = \frac{1}{\delta}\begin{bmatrix} \cos\bar{\alpha}_i & \sin\bar{\alpha}_i \\ -\sin\bar{\alpha}_i & \cos\bar{\alpha}_i \end{bmatrix}\begin{bmatrix} \bar{x}_{i+1} - \bar{x}_i \\ \bar{y}_{i+1} - \bar{y}_i \end{bmatrix}, \tag{17}$$

for $i \in \{1, \ldots, N-1\}$, where δ is the video sampling rate. Similarly, the angular velocity of the MBR can be extracted from the video data by $\bar{\omega}_i = \frac{\bar{\alpha}_{i+1} - \bar{\alpha}_i}{\delta}$.

By equating the averages and the expectations of the MBR's translational and angular velocities, we can estimate

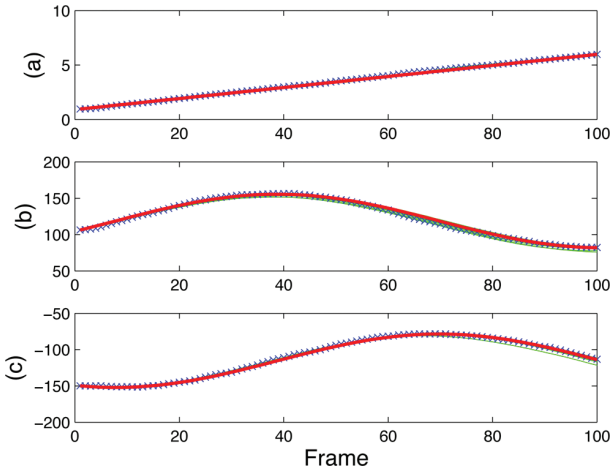

Fig. 7. The comparison between the experimental data (x), the deterministic model prediction (thick line), and stochastic simulations (solid lines) for a rectangular MBR (50 μm × 100 μm). (a) α in rad, (b) x in μm, (c) y in μm.

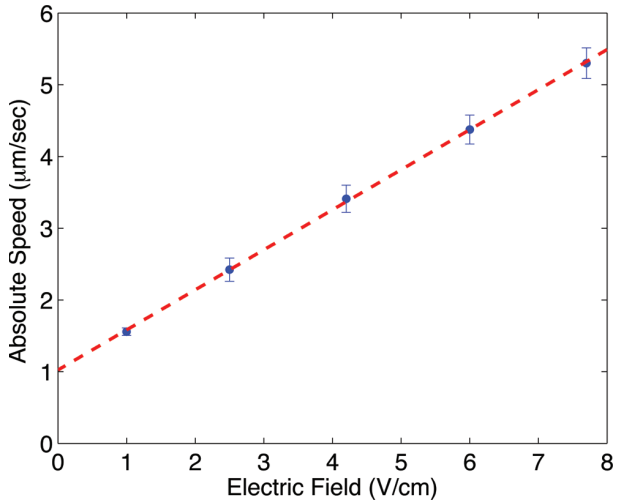

Fig. 8. MBR speed is directly proportional to applied electric field, which shows electrophoresis is the dominant electrokinetic phenomenon. The component of speed due to self actuation appears as an offset along the vertical axis.

the values of $\beta_{1,2,3}$ as follows:

$$\begin{bmatrix} \beta_1 & \beta_2 & \beta_3 \end{bmatrix} \approx \frac{1}{\bar{p}\,(N-1)} \sum_{i=1}^{N-1} \begin{bmatrix} \bar{v}_{x,i} & \bar{v}_{y,i} & \bar{\omega}_i \end{bmatrix}.$$

Figure 6 shows the computed $\{\bar{\omega}_i\}$, $\{\bar{v}_{x,i}\}$, and $\{\bar{v}_{y,i}\}$ for a rectangular MBR (50 μm × 100 μm) as shown in Figure 1. The video length is 100 s, sampled at 1 frame/s. Based on this data, the parameters for this MBR are computed as $\beta_1 = 13.03\ \mu\text{m}/(\text{s pN})$, $\beta_2 = -43.64\ \mu\text{m}/(\text{s pN})$, and $\beta_3 = 1.24\ \text{rad}/(\text{s pN})$.

The three parameters $\beta_{1,2,3}$ summarize the distribution of the bacteria on the MBR. Subsequently, we will show that our mathematical model and the parameters $\beta_{1,2,3}$ can predict the behavior of the system reasonably well.

3.4. Model validation

In this subsection we show that the mathematical model developed in the previous section and the parameters $\beta_{1,2,3}$ can predict the behavior of the system reasonably well. We construct a deterministic model by replacing the stochastic processes $p_i(t)$ in (3) with their steady state expectations $\bar{p}$. We therefore construct a reduced-order model for the system, which is given by

$$\frac{dx}{dt} = \bar{p}\,(\beta_1 \cos\alpha - \beta_2 \sin\alpha),$$

$$\frac{dy}{dt} = \bar{p}\,(\beta_1 \sin\alpha + \beta_2 \cos\alpha),$$

$$\frac{d\alpha}{dt} = \bar{p}\beta_3.$$

Figure 7 shows the comparison between the experimental data, the deterministic model prediction and the stochastic simulations of the model (3) for the rectangular MBR that is analyzed in the previous section. Note that for each simulation run, the distribution of 300 bacteria on the MBR is randomized while keeping the parameters $\beta_{1,2,3}$ constant.

We can see that the model with fitted parameter can explain the data very well. Furthermore, we can observe that the distributed parameter model that includes the description of the distribution of the bacteria on the MBR ($\mathbf{r}_i$ and θ_i) can be replaced with a lumped parameter model with the initial state of the system and three parameters of bacterial distribution ($\beta_{1,2,3}$). Therefore, in order to describe the dynamics of the system accurately, it is not necessary to know how the bacteria are distributed precisely. Rather, it is sufficient to know a few high level parameters that describe the distribution.

4. Model for electrokinetic actuation

The second source of actuation is electrokinetic. Because bacteria are charged, an electric field exerts an electrostatic Coulomb force on the particles. Thus the individual bacteria and therefore the MBR exhibit electrophoresis. In order to develop a model for electrophoresis, two sets of experiments were performed. First, the SU-8 microstructures were tested in the experimental chamber without bacteria attached using DC electric fields ranging from 1 to 10 V/cm. For the electric fields applied during these experiments, the structures demonstrated no movement that might be expected due to electrokinetic effects. In the next set of experiments, electric fields ranging from 1 to 10 V/cm were applied to the MBRs. They responded by immediately seeking the positive electrode with a directed movement that was primarily translational, but also included some rotation because of *self actuation*. Upon switching the polarity of the field, the motion immediately reversed

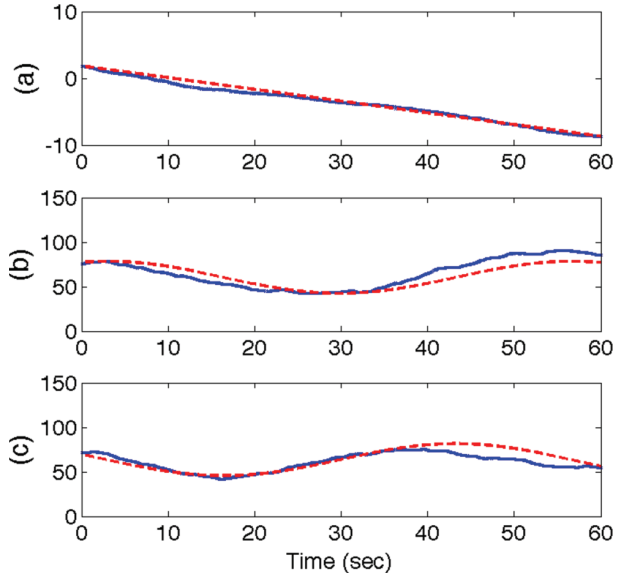

Fig. 9. The comparison between the experimental data (blue line) and the model prediction (red line) for a rectangular MBR (4040 μm × 45 μm) showing self actuation. (a) α in rad, (b) x in μm, (c) y in μm.

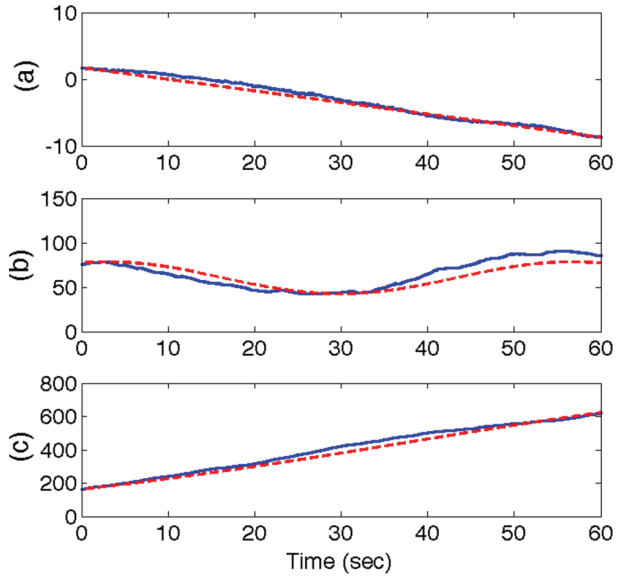

Fig. 10. The comparison between the experimental data (blue line) and the model prediction (red line) for a rectangular MBR (40 μm × 45 μm). 10 V/cm was applied to the MBR in the $+y$ direction. (a) α in rad, (b) x in μm, (c) y in μm.

direction. This investigation yielded a linear relationship between the two parameters reflective of electrophoretic movement (see Figure 8). Thus, the detailed motion of the MBR could be accurately modeled by a sum of the movement due to the self-coordinating, unstimulated movement and electrophoretic movement. Indeed, surface patterning of bacteria imparts a charge that leads to a direct mechanism of translational control of the MBR.

We now extend the model developed in the previous section to incorporate electrokinetic actuation (see Figure 4). If each of the N_b bacteria in the MBR is subject to the same electric field, we arrive at the stochastic kinematic model:

$$\frac{d\mathbf{r}}{dt} = \frac{1}{k_T}\{\sum_{i=1}^{N_b} p_i n_i + N_b(\epsilon_C|E|)\,u\}, \tag{18a}$$

$$\frac{d\alpha}{dt} = \frac{1}{k_R}\{\sum_{i=1}^{N_b} p_i \cdot \left(b_{i,x}\sin\theta_i - b_{i,y}\cos\theta_i\right) + (\epsilon_C|E|)\sum_{i=1}^{N_b}\left(b_{i,x}\sin(\Psi-\alpha) - b_{i,y}\cos(\Psi-\alpha)\right)\}, \tag{18b}$$

where the strength of the electric field is denoted by $|E|$ and u is the unit vector that represents the direction of the electrophoretic force exerted on each bacterium. The strength of the electrophoretic force is given by $\epsilon_C|E|$ where ϵ_C is a constant related to the charge of the cell body.

Experimental observations suggest that the angular velocity of the MBR is not modulated by the application of the electrical fields. In other words, the observed angular velocity with the application of electrical fields was indistinguishable from the angular velocity under self actuation. We conclude that if the whole surface of the MBR is coated with a monolayer of bacteria, the moments due to the applied electric field must be zero. In other words,

$$\sum_{i=1}^{N_b}\left(b_{i,x}\sin(\Psi-\alpha) - b_{i,y}\cos(\Psi-\alpha)\right) = 0. \tag{19}$$

This simplifies the model. The expected velocities can be derived from the stochastic kinematic model:

$$E(v_x) = \beta_1\bar{p} + \beta_4 u_x, \tag{20}$$

$$E(v_y) = \beta_2\bar{p} + \beta_4 u_y, \tag{21}$$

$$E(\omega) = \beta_3\bar{p}, \tag{22}$$

where $\beta_4 = (1/k_T)N_b\epsilon_C$ is experimentally determined via linear regression from experimental data (see Figure 8).

The comparison of the experimental observations with theoretical predictions is shown for a representative experiment in Figure 9 and Figure 10 with a 40×45 μm^2 rectangular MBR with the parameters $\beta_1 = -6 \times 10^{12}$ μm/(s N), $\beta_2 = -5 \times 10^{12}$ μm/(s N), $\beta_3 = -0.43 \times 10^{12}$ rad/(s N), and $\beta_4 = 0.56 \times 10^4$ μm^2/(s V). In the first part of the experiment, we recorded a video of the motion of the MBR in the absence of external stimuli showing motility due to self actuation. We estimated the values of $\beta_{1,2,3}$ using the processed data as described in the previous section. Compared to the match we obtained (see Figure 7) for the larger rectangular MBR given in Figure 1, there is more discrepancy between experimental data and simulation results. As the

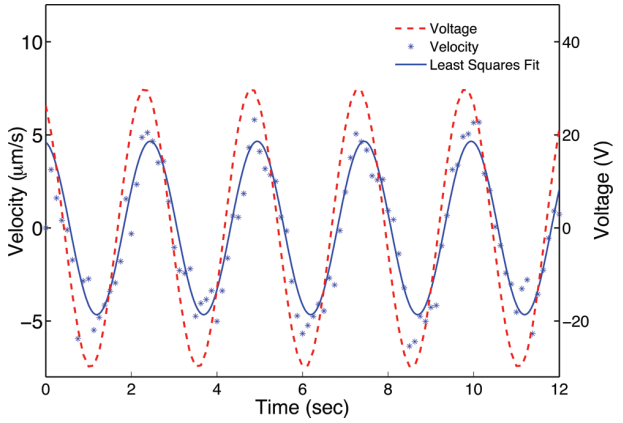

Fig. 11. The velocity of a 20×22 μm^2 rectangular MBR as a response to a sinusoidal input voltage (dashed line) with an amplitude of 30 V and a frequency of 0.4 Hz. A least squares minimization was used to fit a sine curve (solid line) representing the velocity data (*).

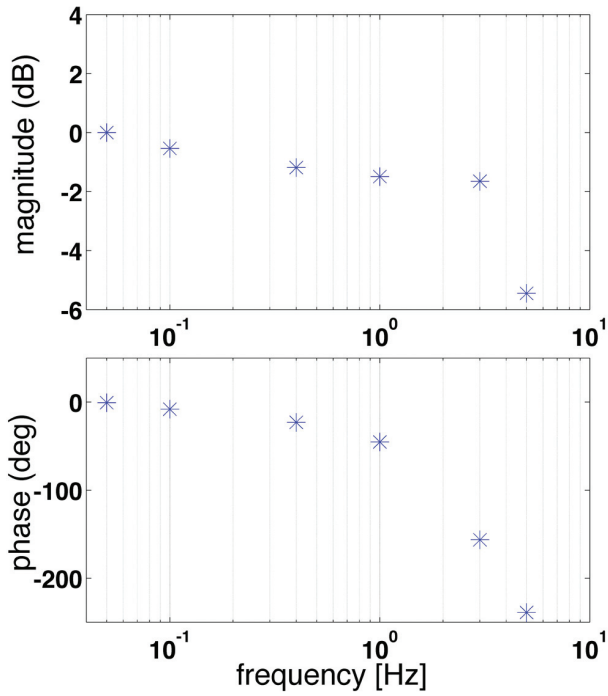

Fig. 12. Bode plot of the system.

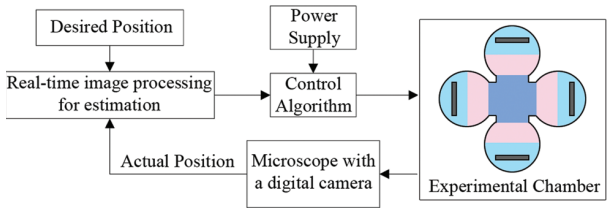

Fig. 13. Block diagram for vision-based computer control of MBRs. The vision system informs the control algorithm of the current position of the robot. The control algorithm calculates the distance between the current and the desired positions and finds the power supply voltages that will create the electric field required to steer the robot towards its next destination.

number of random actuators decreases, the motion of the MBR becomes more unpredictable. A small change in the orientation of one of the bacterium would cause an observable change in the overall MBR motion if the applied force by this bacterium is comparable to the net force acting on the robot. This change could be due to loose attachment of the bacterium. We fabricated smaller microstructures with sizes less than 10 μm and they showed even more erratic behavior.

During the second part of the experiment, 10 V/cm was applied to the MBR in the $+y$ direction. There was no significant variation in the angular velocity or the translational velocity in the x direction as expected. The observed difference could be initiated by galvanotaxis, a directed response arising from the thrust of the bacterial flagella. Galvanotaxis in bacteria is caused by a difference in electrophoretic mobility between the cell body and flagellum (Shi et al., 1996). The MBR moved with a constant velocity of 7 μm/s in the $+y$ direction. The electrokinetic model with the fitted parameters can explain the data well, suggesting that the overall structure of the model is suitable for this system.

5. System characterization

The entire MBR system incorporates several elements that have not been previously characterized in great detail. These elements include the electrokinetic response of groups of cells attached to microfabricated structures, the movement of microscale plates along substrates in fluidic environments, and the electronic response of agar-based galvanotactic control chambers at relatively high switching frequencies.

As such, a system characterization was performed to accomplish several objectives. Primarily, the characterization was performed to understand the overall dynamic response and, in turn, the degree of controllability of the MBR system. Additionally, the characterization results lend insight to future experimental design. In particular, knowledge of the dynamic response is useful for determining video sampling rates and computational requirements. The characterization is also necessary to test the feasibility of using electrokinetic actuation for applications like microassembly, and to lay groundwork for the optimization of controller design.

To characterize the electrokinetic response of the system, a series of trials were run with a sinusoidal control voltage with amplitude of 30 V. The frequency was varied from 0.05 to 5 Hz in one direction. The MBRs were tracked with subpixel resolution to determine velocity, which is directly related to voltage through the relation for electrophoresis

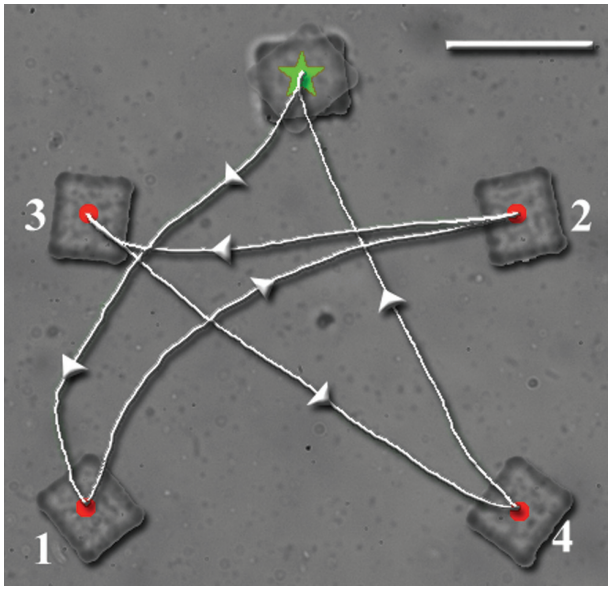

Fig. 14. Steering of a 20×22 μm^2 rectangular MBR along a star-shaped path. The MBR passes through destinations 1–4 before stopping at its initial position. The scale bar represents 50 μm.

given in (18). As such, the response of the system was determined by using the amplitude of the sinusoidal velocity. Since the self-actuation component of MBR motion causes deviation from the purely electrokinetic component, a least squares minimization was used to fit the sine curves at each frequency (Figure 11). The curve fit was applied only after the steady state was achieved. The least squares fit routine additionally smooths the noise that is introduced in the tracking algorithm. The tracking noise arises due to fluctuations in light intensity and movements of individual bacteria along the edges of MBRs. The MBR followed the input signal quite well up to a cutoff frequency near 3 Hz, where the magnitude dropped off considerably (Figure 12). At 3 Hz, the phase lag increased to 2.73 rad.

Due to the dominance of viscous forces at such small length scales, inertial effects would typically be expected to be negligible at the tested frequencies. Thus, other sources for the loss of phase coherence and drop in magnitude should be considered. The electrochemical circuitry of the experimental chamber includes buffer solutions and agar electrodes, and charging effects may play a role in the observed changes in response around 3 Hz.

6. Control of MBRs

6.1. Control law and feedback

The basic feedback control steering concept is described in Figure 13. Even a simple control algorithm is sufficient to steer our MBRs. The desired goal can be accomplished using one of two approaches.

If the desired trajectory $r^{\text{des}}(t)$ is given, then the applied electric field can be adjusted with a simple proportional control law:

$$U = K(r^{\text{des}} - r) + \dot{r}^{\text{des}}, \tag{23}$$

where K is a suitable positive constant and $\dot{r}^{\text{des}}$ is the feedforward term. In the presence of *self actuation*, the error $e = r^{\text{des}} - r$ cannot be driven to zero. However, the error can be predicted accurately using the mathematical model in (7)–(11).

We employed an alternative solution in which we fixed the speed of the MBR and only controlled the direction of motion. This time, instead of having the desired trajectory, we define a series of target points. The control law is given by

$$U = \frac{K(r^{\text{des}} - r)}{\|r^{\text{des}} - r\|}. \tag{24}$$

6.2. Results

As a demonstration, a star-shaped trajectory was defined by choosing five destination points corresponding to the corners of the star (see Figure 14). These target locations were fed to the feedback control algorithm that uses the current location of the MBR and the position of the next destination to control the applied voltage. The real-time image processing algorithm processes the captured frames and the control algorithm updates the applied voltages with a frequency of 8 Hz (see video Extension 1).

The star-shaped trajectory experiment demonstrates a number of capabilities of the MBR system. First, the experiment demonstrates the ability to locate the centroid of the MBR to single pixel resolution (0.5 μm). Additionally, the experiment demonstrates the ability to quickly switch directions and to follow arbitrary slopes with only four electrodes and two amplifiers.

The overall trajectory followed by a 20×22 μm^2 rectangular MBR is given in Figure 14. The MBR successfully passed through all the predetermined destination points. The robot immediately responded to the changes in the applied voltage thanks to the absence of inertia at low Reynolds number, and its velocity followed a similar trend with the applied voltage as expected (see Figure 15).

Before running the control algorithm, $\beta_{1,2,3}$ were estimated as described in Section 3. The values of the parameters were found to be $\beta_1 = -0.2 \times 10^{12}$ μm/(s N), $\beta_2 = 0.65 \times 10^{12}$ μm/(s N), $\beta_3 = -0.28 \times 10^{12}$ rad/(s N), and $\beta_4 = 0.56 \times 10^4$ μm^2/(s V). We imported the voltage input applied during the experiment (see Figure 15) to the mathematical model and simulated the response of the MBR described by the estimated parameters. The comparison of the experimental observations with theoretical predictions is shown in Figure 16. Even though the control input changes continuously, the predicted trajectory closely resembles the observed one with an average deviation less than 20 μm.

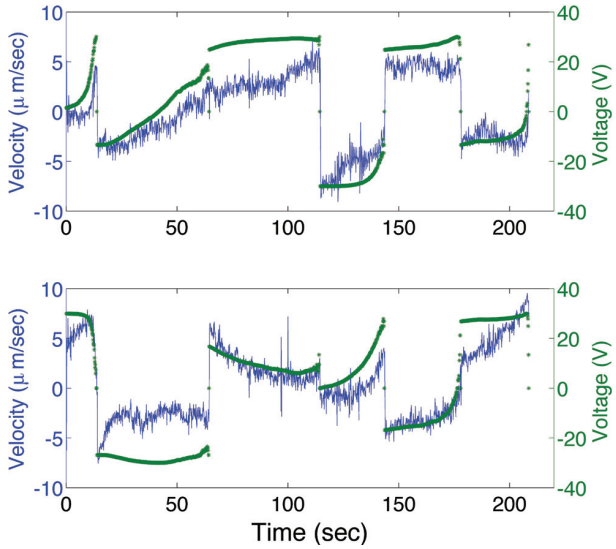

Fig. 15. The voltage applied to the system and the corresponding velocity of the MBR in x (top) and y (bottom) directions during the experiment. The robot responded to the changes in voltage immediately as expected.

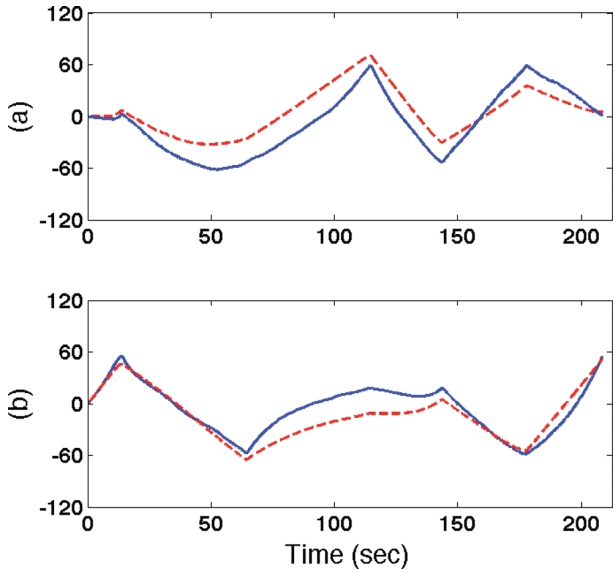

Fig. 16. The comparison between the experimental data (blue line) and the model prediction (red line) for the star experiment. (a) x in μm, (b) y in μm.

By increasing the number of destination points, we could be able to decrease the tracking error. A 20×22 μm^2 rectangular MBR successfully followed first a circular and then a diamond shaped trajectory (Figure 17).

7. Discussion

One shortcoming of the model that may explain the slight deviation in terms of linear velocities between predictions and experiments is our implicit assumption of symmetry when calculating the drag force. Our drag coefficients k_T and k_R are independent of the orientation of the MBR. We are currently developing a numerical analysis of the drag force acting on a rectangular plate moving parallel to a surface in a low Reynolds number regime and this may yield an even better match with the data. This analysis would also lead us to estimate the force required to move the microstructures with certain speeds. An alternative method for quantifying the drag coefficients is to apply a known force using an Atomic Force Microscope and then measure the corresponding speed of the microstructure. A force sensor could also be used, although the sensor would need to be extremely sensitive as the total force applied is in the order of piconewtons.

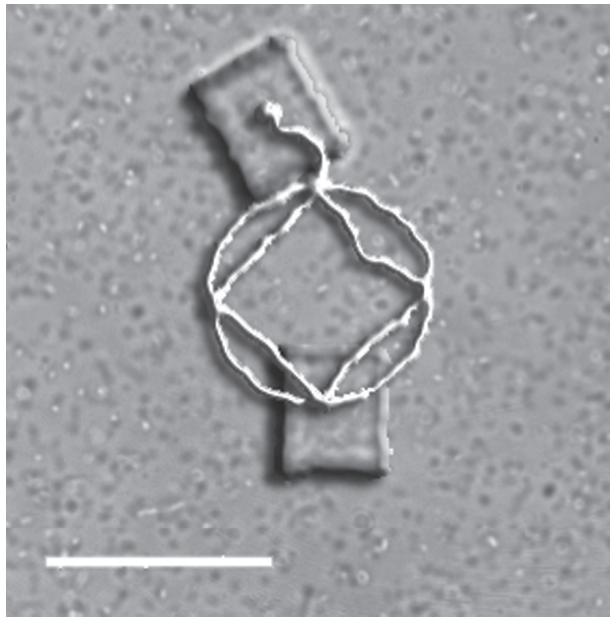

Fig. 17. Steering of a 20×22 μm^2 rectangular MBR along a circular and a diamond shaped path. The MBR passes through the destinations and returns to its original position. The scale bar represents 50 μm.

We do not measure the electrophoretic mobility of the bacteria or the individual robots. Yet the estimated value of β_4 is good enough to predict the average effect of electric fields on the motion of MBRs. By making an on-line measurement of β_4 for each MBR during the steering experiments, a better controller for the electrokinetic actuation could be obtained. The mathematical model can also be incorporated into the control algorithm as a predictive tool to improve the overall accuracy. The current experimental setup does not allow us to control the distribution of the attached bacteria. However, in our future work, we plan to explore different techniques to control the position and orientation of the cells before, during and after attachment. It has been shown that motility of microrobots could be enhanced by selectively patterning cells on specific sites (Behkam and Sitti, 2008).

Most of the movement arises from the applied electric field, so the motivation for having living cells may seem

unclear. As an alternative approach, we coated the surface of SU-8 microstructures with a silane that is positively charged due to the linked carboxyl groups. However, the microstructures stopped moving as if they lost their charges soon after we started applying electric fields. This could be due to the changes caused by ionic exchange inside the fluidic chamber, which should be investigated further. On the other hand, the bacteria cells preserve their charge throughout the experiment at different electric field strengths, an essential property needed to model and control their motion. Another advantage is that bacteria can be used as on-board biosensors. We previously described the development of biosensors for the MBRs (Sakar et al., 2010a). This was done by attaching genetically engineered *Escherichia coli* cells that were capable of sensing non-metabolizable lactose analog methyl-β-D-thiogalactoside (TMG). The bacteria can sense chemicals in the environment and produce fluorescent proteins (GFP) in response, and fluorescent microscopy was used to estimate the chemical concentration in the environment.This immediately points to the feasibility of using estimates of GFP activity combined with electrokinetic actuation to steer MBRs toward biochemical sources.

The control capabilities of the MBRs can be extended by patterning cells on different parts of microstructures. Thanks to a nonuniform distribution of charges, the angular velocity of the MBRs will become controllable using electric fields. It has been shown that a selective patterning of living bacteria can be generated by using a microcontact printing process (Cerf et al., 2008). Furthermore, exposure to ultraviolet (UV) light has been established as a mechanism which affects the motility of bacteria (Taylor and Koshland, 1975). Since MBRs are self-actuated in the absence of external stimuli, use of UV light exposure is an effective means of stopping the motion due to self actuation (Steager et al., 2007). The bacterial flagella gradually de-energize during exposure while the magnitude of the angular velocity of the MBRs decreases exponentially. This characterization could be used to adjust the angular orientation of MBRs.

Finally, in our previous work, we presented the construction and operation of micrometer-sized, biocompatible ferromagnetic microtransporters driven by external magnetic fields (Sakar et al., 2010b). The ferromagnetic photoresist was prepared by mixing iron oxide nanoparticles with the photoresist (SU-8) we used in this study. By attaching bacteria on this composite substrate, we are planning to control our robots using both electric and magnetic fields, and to employ bacteria as biosensing elements.

8. Conclusion

In this paper, several important experimental techniques for building *MicroBioRobots* (MBRs) are proposed and a theoretical framework for modeling and control of MBRs is presented. In particular, we proposed a method of controlling MBRs using self actuation and DC electric fields, and developed an experimentally validated mathematical model for MBRs. We demonstrated experimentally that vision-based feedback control allows a four-electrode experimental device to steer MBRs along arbitrary paths with micrometer precision. At each time instant, the system identifies the current location of the robot, a control algorithm determines the power supply voltages that will move the charged robot from its current location toward its next desired position, and the necessary electric field is then created.

The results presented in this paper have great potential. Our techniques can be used to fabricate, calibrate and transport MBRs in microfluidic channels in a controllable fashion. We are also planning to accomplish micromanipulation and microassembly tasks using our MBRs. Our future work will also address the integration of biosensing and bio-actuation onto MBRs.

Funding

This work was partially supported by the National Science Foundation CAREER (grant numbers CMMI-0745019 and CBET-0828167) and ARO MURI SWARMS (grant number W911NF).

Conflict of Interest

The authors declare that they have no conflicts of interest.

References

Alberti L and Harshey R (1990) Differentiation of serratia marcescens 274 into swimmer and swarmer cells. *Journal of Bacteriology* 172(8): 4322–4328.

Behkam B and Sitti M (2007) Bacterial flagella-based propulsion and on/off motion control of microscale objects. *Applied Physics Letters* 90:023902.

Behkam B and Sitti M (2008) Effect of quantity and configuration of attached bacteria on bacterial propulsion of microbeads. *Applied Physics Letters* 93:223901.

Berg H (2000) Motile behavior of bacteria. *Physics Today* 53(1): 24–29.

Cassandras C and Lafortune S (1999) *Introduction to Discrete Event Systems*. Dordrecht: Kluwer.

Cerf A, Cau J-C and Vieu C (2008) Controlled assembly of bacteria on chemical patterns using soft lithography. *Colloids and Surfaces B: Biointerfaces* 65: 285–291.

Chang S, Paunov V, Petsev D and Velev O (2007) Remotely contolled self-propelling particles and micropumps based on miniature diodes. *Nature Materials* 6: 235–240.

Darnton N, Turner L, Breuer K and Berg H (2004) Moving fluid with bacterial carpets. *Biophysical Journal* 86: 1863–1870.

Darnton N, Turner L, Rojevsky S and Berg H (2007) On torque and tumbling in swimming Escherichia coli. *Journal of Bacteriology* 189: 1756–1764.

Dauge M, Gauthier M and Piat E (2007) Modelling of a planar magnetic micropusher for biological cell manipulations. *Sensors and Actuators A* 138: 239–247.

Donald B, Levey C and Paprotny I (2008) Planar microassembly by parallel actuation of mems microrobots. *Journal of Microelectromechanical Systems* 17: 789–808.

Dreyfus R, Roper M, Stone H and Bibette J (2005) Microscopic artificial swimmers. *Nature* 437: 862–865.

Feinberg A, Feigel A, Shevkoplyas S, Sheehy S, Whitesides G and Parker K (2007) Muscular thin films for building actuators and powering devices. *Science* 317: 1366–1370.

Ghosh A and Fischer P (2009) Controlled propulsion of artificial magnetic nanostructured propellers. *Nano Letters* 9: 2243–2245.

Henrichsen J (1972) Bacterial surface translocation: a survey and a classification. *Bacteriology Reviews* 36(4): 478–503.

Hiratsuka Y, Miyata M, Tada T and Uyeda T (2006) A microrotary motor powered by bacteria. *Proceedings of the National Academy of Sciences* 103: 13618–13623.

Jager E, Inganas O and Lundstrom I (2000) Microrobots for micrometer-size objects in aqueous media: potential tools for single-cell manipulation. *Science* 288: 2335–2338.

Julius A, Sakar M, Steager E, Cheang U, Kim M, Kumar V and Pappas G (2009) Harnessing bacterial power in microscale actuation. In: *IEEE International Conference on Robotics and Automation*, Kobe, Japan, 1004–1009.

Leong T, Randall C, Benson B, Bassik N, Stern G and Gracias D (2009) Thetherless thermobiochemically actuated microgrippers. *Proceedings of the National Academy of Sciences* 106(3): 703–708.

Linder V, Gates B, Ryan D, Parviz B and Whitesides G (2005) Water-soluble sacrificial layers for surface micromachining. *Small* 7: 730–736.

Martel S, Tremblay C, Ngakeng S and Langlois G (2006) Controlled manipulation and actuation of micro-objects with magnetotactic bacteria. *Applied Physics Letters* 89:233904.

Pawashe C, Floyd S and Sitti M (2009) Multiple magnetic microrobot control using electrostatic anchoring. *Applied Physics Letters* 94: 164108.

Sakar M, Steager E, Kim D, Julius A, Kim M, Kumar V and Pappas G (2010a) Biosensing and actuation for microbiorobots. In: *IEEE International Conference on Robotics and Automation*, Anchorage, AL, 3141–3146.

Sakar M, Steager E, Kim D, Kim M, Pappas G and Kumar V (2010b) Single cell manipulation using ferromagnetic composite microtransporters. *Applied Physics Letters* 96: 043705.

Shi W, Stocker B and Adler J (1996) Effect of surface composition of motile e.coli and motile salmonella on the direction of galvanotaxis. *Journal of Bacteriology* 178: 1113–1119.

Sokolov A, Apodaca M, Grzybowski B and Aranson I (2010) Swimming bacteria power microscopic gears. *Proceedings of the National Academy of Sciences* 107: 969–974.

Song B, Gu Y, Pu J, Reid B, Zhoa Z and Zhao M (2007) Application of direct current electric fields to cells and tissues in vitro and modulation of wound electric field in vivo. *Nature Protocols* 2: 1479–1489.

Steager E, Kim C-B, Naik C, Patel J, Bith S, Reber L, et al. (2007) Control of microfabricated structures powered by flagellated bacteria using phototaxis. *Applied Physics Letters* 90: 263901.

Tandon N, Cannizzaro C, Chao P-H, Maidhof R, Marsano A, Au H, et al. (2009) Electrical stimulation systems for cardiac tissue engineering. *Nature Protocols* 4: 155–173.

Taylor B and Koshland D (1975) Intrinsic and extrinsic light responses of salmonella typhimurium and escherischia coli. *Journal of Bacteriology* 123: 557–569.

Ueda J, Odhner L and Asada H (2007) Broadcast feedback of stochastic cellular actuators inspired by biological muscle control. *International Journal of Robotics Research* 26(11): 1251–1266.

van den Heuvel M and Dekker C (2007) Motor proteins at work for nanotechnology. *Science* 317: 333–336.

Vollmers K, Frutiger D, Kratochvil B and Nelson B (2008) Wireless resonant magnetic microactuator for untethered mobile microrobots. *Applied Physics Letters* 92: 144103.

Weibel D, Garstecki P, Ryan D, DiLuzio W, Mayer M, Seto J, et al. (2005) Microoxen: Microorganisms to move microscale loads. *Proceedings of the National Academy of Sciences* 102: 11963–11967.

Zhang L, Abbott J, Dong L, Kratochvil B, Bell D and Nelson B (2009) Artificial bacterial flagella: Fabrication and magnetic control. *Applied Physics Letters* 94: 064107.

Appendix A: Index to Multimedia Extensions

The multimedia extension page is found at http://www.ijrr.org.

Extension	Type	Description
1	Video	Vision-based computer control of MBRs